JTTEE5 14:117-124
DOI: 10.1361/10599630522675
1059-9630/$19.00 © ASM International

In-Flight Oxidation of Stainless Steel Particles in Plasma Spraying

A.A. Syed, A. Denoirjean, P. Denoirjean, J.C. Labbe, and P. Fauchais

(Submitted September 3, 2003; in revised form March 30, 2004)

Air engulfment by the plasma jet in air plasma spraying (APS) causes in-flight oxidation of metallic particles. This oxidation, often complex and difficult to explain by classic diffusion-controlled oxidation, is governed by several mechanisms. This paper highlights the possible in-flight oxidation mechanisms in metallic particles with a focus on the convective oxidation. Two different types of austenitic stainless steel particles were air plasma sprayed using a direct current plasma gun and were collected in an argon atmosphere. Preliminary experiments indicated that different mechanisms are likely to occur during the in-flight oxidation of particles. The mass transfer from surface to interior of particle occurred, forming oxide nodules within particles. The mass transfer is governed by convective movements inside liquid particles within the plasma jet core due to the plasma-particle kinematic viscosity ratio greater than 50 and particle Reynolds number (Re) higher than 20. The nodules were composed of metastable phases consisting of mixed oxide of Fe and Cr. Convective movements within particles ceased roughly outside of the plasma jet core, and classic surface oxidation was found to be the dominant phenomenon forming the surface oxide layer. Moreover, the molten surface oxide outside the jet core may become entrained toward the tail of the particle if plasma conditions promote a higher particle Re number. The major oxide phase in collected particles was $FeCr_2O_4$, in a nonstoichiometric form of $Fe_{3-x}Cr_xO_4$.

Keywords convective reactivity, in-flight oxidation, LECO, Mössbauer spectroscopy, plasma

1. Introduction

When spraying fully melted metallic particles, in most cases heated much over their melting temperature, fast chemical reactions may occur even if their residence time in the reacting zone is a few milliseconds at the maximum. In-flight oxidation of metal particles occurs in atmospheric plasma spraying (APS) (Ref 1) due to the entrainment of the surrounding air into the plasma jet (Ref 2). It is, therefore, common to find oxide phases in APS metal coatings (Ref 3). Air entrainment occurs both by the engulfment process at plasma jet-air boundary and plasma jet fluctuations (Ref 4, 5). The velocity distribution of the plasma jet and its viscosity, through the composition of plasma forming gases, influence the quantity of entrained surrounding atmosphere (Ref 6, 7). In-flight oxidation of sprayed particles begins due to gas-solid interaction during heating of particles to their melting point in the plasma. In molten particles, oxidation rate increases with a gas-liquid interaction through diffusion and convection. A gas-solid interaction may occur if the particles resolidify within the plasma jet (Ref 8, 9). The in-flight oxidation, often resulting in metastable oxides, was initially suggested to be diffusion-controlled phenomenon. Sobolev and Guilemany (Ref 10) have proposed that intensive motion of liquid phase can increase the coefficient of diffusion and a high percentage of oxygen can get dissolved in the particle. Other studies, however, found the oxide amount present within collected particles too high to be explained by diffusion models (Ref 11, 12).

Oxides in coatings are considered to influence the structure and properties of deposits (Ref 13, 14). Many authors have reported detrimental effects of accompanied oxide in metallic deposits (Ref 15, 16). These oxides, however, can result in improved properties such as higher wear resistance (Ref 17), superior compressive strength (Ref 18), and better adhesion due to the improved wettability of oxidized particles (Ref 19). Recently, Syed et al. (Ref 20) have shown that in-flight oxidation is a multistage phenomenon, and oxidation may be governed by different mechanisms.

In the present work, the oxide formation during air plasma spraying 316L austenitic stainless steel was studied, and the particle oxidation mechanisms in the plasma jet core and plasma plume were investigated.

2. Experimental Technique

Two 316L austenitic stainless steel powders, one commercially named 41C (−106 +45 μm) from Sulzer Metco, USA and the other grade TY316L (−63 +50 μm) from Techphy Groupe H.T.M., France, were sprayed using a direct current (dc) plasma gun (PTF4 type) with a 7 mm internal diameter (ID) anode nozzle. In some other experiments, an anode with 6 mm ID was used. The former powder was produced by a water atomization process and the latter by a gas atomization technique (see Fig. 1 showing their morphologies). The chemical compositions of both powders are given in Table 1.

The original version of this article was published as part of the ASM Proceedings, *Thermal Spray 2003: Advancing the Science and Applying the Technology*, International Thermal Spray Conference (Orlando, FL), May 5-8, 2003, Basil R. Marple and Christian Moreau, Ed., ASM International, 2003.

A.A. Syed, A. Denoirjean, P. Denoirjean, J.C. Labbe, and **P. Fauchais,** SPCTS, Faculté des Sciences, Université de Limoges, Limoges, France. Contact e-mail: asif.syed@dlr.de.

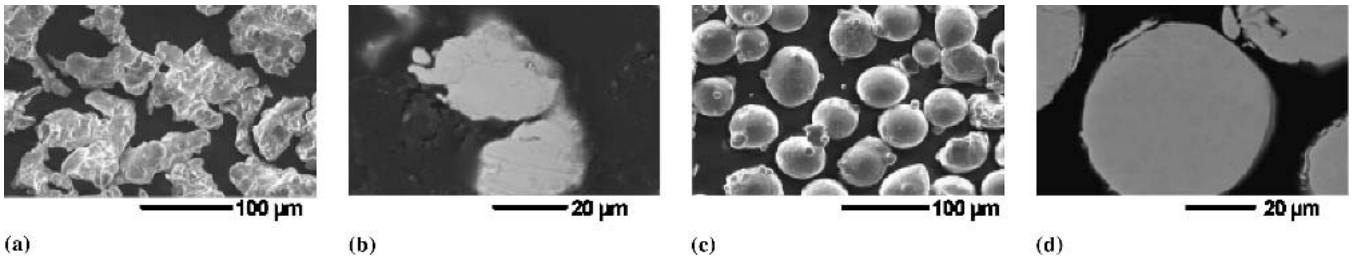

Fig. 1 Micrographs of feedstock 316L stainless steel particles. Surface (a) and cross section (b) of Metco powder; and surface (c) and cross section (d) of Techphy powder

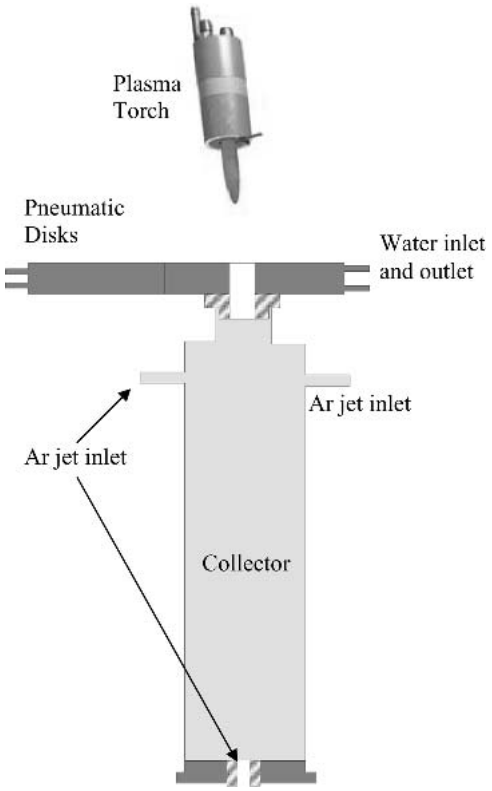

Fig. 2 In-flight powder collection setup

Table 1 Composition of feedstock 316 austenitic stainless steel powders

	Composition, wt.%						
	Cr	Ni	Mo	Mn	Si	C	Fe
Metco 41C	17	12	2.5	…	1	0.1	bal
Techphy TY316L	19	11	2.4	1.2	0.4	0.01	bal

Table 2 Oxygen content in feedstock powders by LECO

	Feedstock Techphy	Feedstock Metco
Oxygen content, wt.%	0.030 ± 0.003	0.143 ± 0.008

In all experiments, the arc current was 550 A and the plasma gas flow consisted of 45 slm (80.25 g/min) Ar and 15 slm (1.34 g/min) H_2, resulting in an electric power output of 33 kW

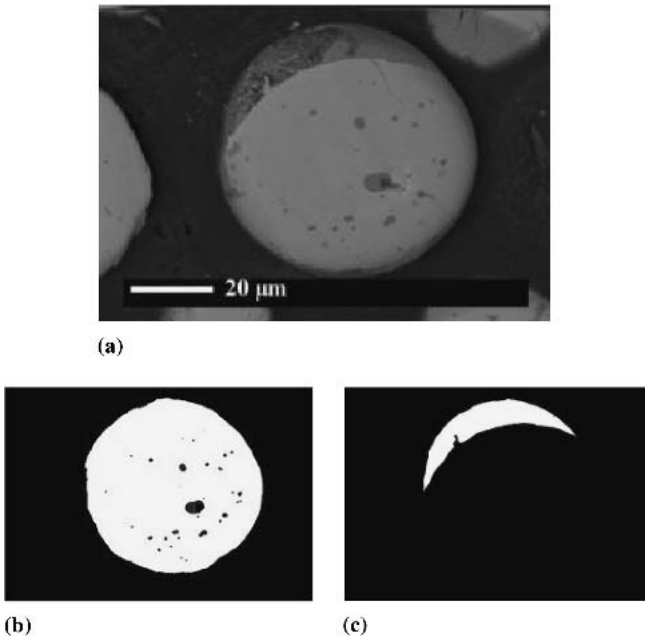

Fig. 3 Image treatment analysis of (a) the polished cross sections of a collected particle, (b) measurements of oxide nodules, and (c) oxide cap

and a thermal efficiency of 56%. This plasma gas mixture was probably too energetic with a high heat transfer coefficient for the selected powder. However, this made it possible to enhance the in-flight particle oxidation, thus allowing precise analysis of the oxide content of collected particles and a better understanding of their oxidation mechanisms.

Powders were sprayed and collected in a cylindrical collector 650 mm in height and 130 mm in diameter, with the standoff distance of the collector varied between 50 and 100 mm. A water-cooled double-disk pneumatic system was disposed at the top of the cylinder. One of the two disks, with an aperture of 22 mm, was centered in the middle of the sprayed spot, whereas the other disk was fabricated without any opening. The disks were moved over the cylinder by a pneumatic system allowing or blocking the powder passage into the collector. The particles entering the collector were quenched by argon jets flowing through four inlets, three fixed at the collector entrance and one introduced at the bottom. The former favored rapid quenching of the particles, whereas the latter helped in their deceleration besides their continuous cooling. Argon flow rate was optimized around at 60 slm. The measured quenching rate of particles in

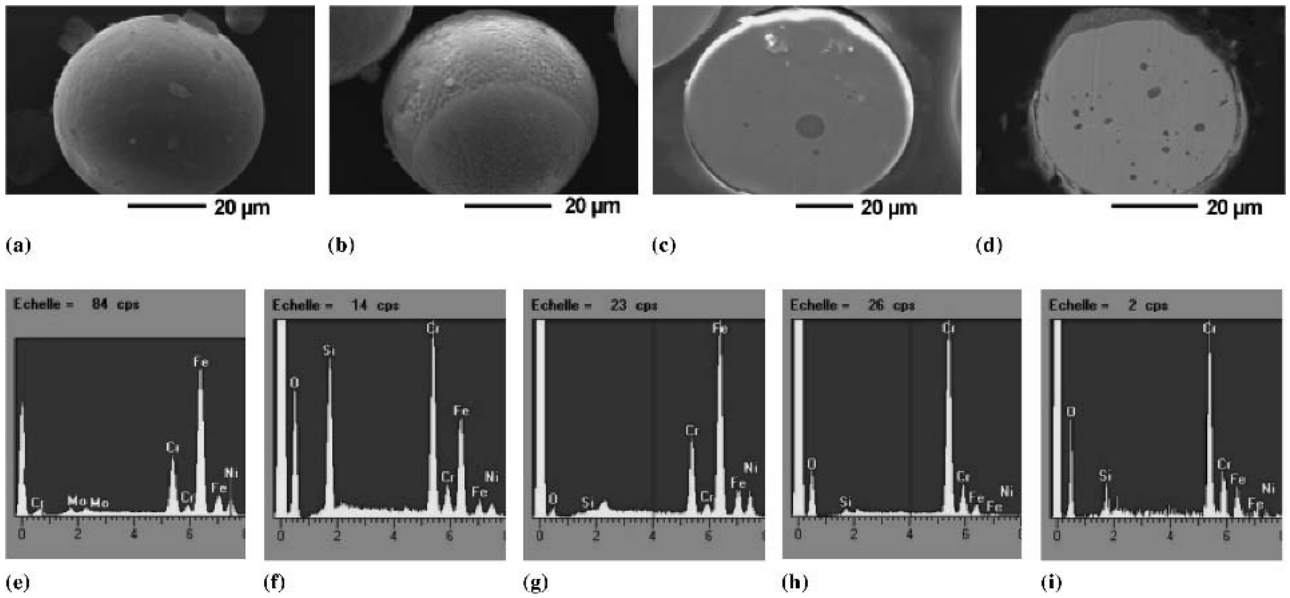

Fig. 4 Micrographs of collected oxidized particles: surface of (a) Metco and (b) Techphy particles and cross section of (c) Metco and (d) Techphy particles. EDS analysis: (e) base metal, (f) surface of collected Metco particle, (g) coarse-grained layer covering Techphy particle, (h) oxide cap in the Techphy particle, and (i) island of oxide nodule in Techphy particle. The oxide nodule in Metco particle revealed EDS analysis similar to (i).

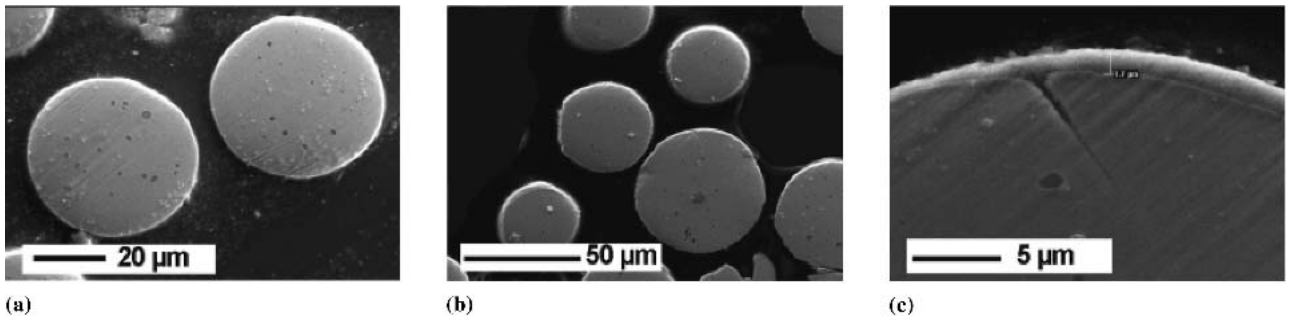

Fig. 5 Techphy 316L particles collected at (a) 50 mm and (b) and (c) 75 mm after air plasma spraying (I = 550 A, Ar-H_2 = 45 to 15 slm, anode nozzle ID = 7 mm)

the collector approached 5 ×10^6 K/s, which was lower than that estimated during initial stages of splat cooling (10^8 K/s) on substrate surface (Ref 21, 22). A schematic illustration of the collection setup is shown in Fig. 2.

Global oxygen content in feedstock and collected particles was determined using an "extractive fusion" technique (LECO, USA). A Philips XL 30 scanning electron microscope (SEM) was used to obtain micrographs that were later used for statistical measurements of oxide nodules and total oxide surface area percentages by image treatment analysis (Fig. 3). The elemental analyses were performed by EDX 9100/60 energy dispersive spectroscopy (EDS) and more precisely by electron microprobe analysis (EMPA). Different techniques including x-ray diffraction (XRD), Fourier transform infrared (FTIR) spectroscopy, and Mössbauer spectroscopy were used for phase analyses. A Siemens D500 diffractometer using a copper anode was used for XRD, and a Nicolet 710 equipped with a Michelson interferometer was used to obtain FTIR spectra. ^{57}Fe Mössbauer spectroscopy of samples was conducted using a ^{57}Co radioactive source fixed in an Rh matrix.

3. Results and Discussion

The feedstock steel powders exhibited some residual oxygen (Table 2) that could be due to the oxygen dissolved in the metal and/or accumulated as thin oxide layer on particles surface. Oxides were not observed within particles, as can be seen in Fig. 1(b) and (d). Spherical collected particles after spraying (Fig. 4a and b) were composed of an outer layer rich in oxygen along with Cr, Fe, and Si. The Si peak was particularly high in the collected Metco particle (Fig. 4f), as Si content of feedstock Metco powder was much higher than that of Techphy powder. The outer layer can be considered the oxide formed on the surface of particles within the plasma jet. A uniform surface can be

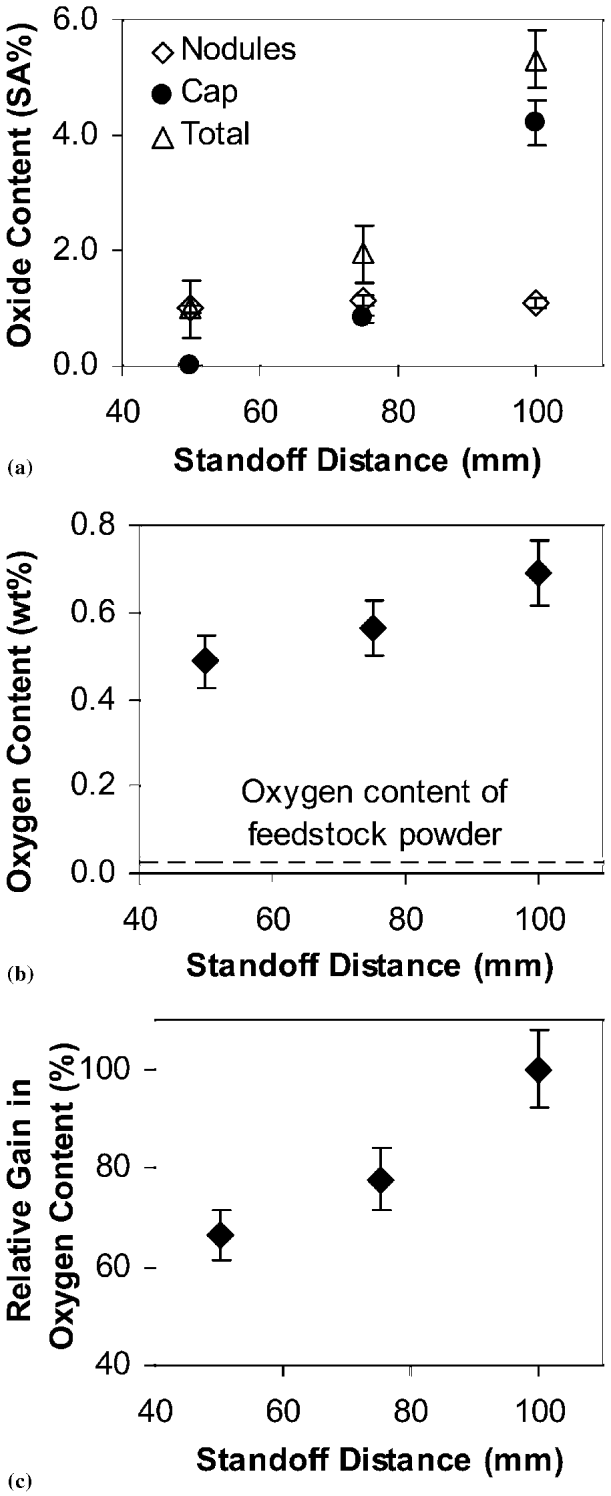

Fig. 6 Oxide and oxygen content data in the collected Techphy particles. (a) Percentage of surface area (SA%) of oxides after image treatment analysis. (b) Oxygen mass content after LECO. (c) Change in oxygen mass fraction relative to the oxygen content of powder collected at 100 mm standoff distance

observed for collected Metco particles (Fig. 4a), contrary to collected Techphy particles (Fig. 4b), where the outer layer can be distinguished as a fine-grained cap covering a fraction of the particle surface and a coarser-grained secondary layer covering the rest of the particle.

The difference in the microstructure can be an indication of a possible difference either in the type of oxide or in the formation mechanism. EDS showed that the coarse layer had a composition closer to that of feedstock Techphy powder, though a weaker oxygen peak was detected (Fig. 4g). The cap area was, however, rich in chromium and oxygen. A weak Fe peak and an absence of Ni were also indicated (Fig. 4h).

The cross sections of collected particles (Fig. 4c and d) present two distinct phases: a brighter area and more or less spherical darker nodules. The oxide cap and the thin layer covering the rest of the Techphy particle can also be observed in Fig. 4(d). The EDS analysis illustrates that the brighter area is the base metal (Fig. 4e), whereas nodules are composed of mainly oxygen and Cr along with Si and Fe (Fig. 4i). The cap exhibits similar elemental analysis than that of the nodule (Fig. 4h). The following section gives an account of the phenomena resulting in formation of oxide nodules and cap. Details of elemental and phase analysis in collected particles are discussed toward the end of the article.

Techphy particles were collected varying the standoff distance between 50 and 75 mm from the torch. No oxide cap were observed in particles collected at 50 mm standoff distance as it can be seen in Fig. 5(a),whereas at 75 mm, particles with only thin caps were collected (Fig. 5b and c). After image treatment analysis, it was found that the surface area percentage of oxide nodule did not vary significantly after 50 mm, whereas the surface area percentage of oxide cap and thus total oxide increased with an increasing distance from 50 to 100 mm (Fig. 6a). Though the oxide formed at surface starts segregating in the cap form between 50 and 75 mm standoff distance in Techphy particles, major oxide segregation occured between 75 and 100 mm standoff distance of plasma jet exit.

The oxygen content in collected Techphy particles increased linearly between 50 and 100 mm standoff distance (Fig. 6b) with major oxidation taking place within the first 50 mm. Oxygen mass percentage of particles collected at 50 mm standoff distance corresponds to 67% of that present in particles at 100 mm (Fig. 6c).

The difference between liquid drop and surrounding media kinematic viscosities ($\upsilon = \mu/\rho$; μ is dynamic viscosity; ρ is specific mass) and particle Reynolds number (Re) can result in convective movements within the drop (Ref 23, 24) forming a spherical hill vortex (Ref 25). These conditions are expected within the plasma jet core where the plasma to particle kinematic viscosities ratio ($\upsilon_i = \upsilon_{plasma}/\upsilon_{particle}$) is often >50 and particle Re is >20 (Ref 26). Surface structure in the micrographs of particles collected at 50 mm standoff distance (Fig. 7) also gave evidence of possible convective movements. The oxide formed and the oxygen dissolved at the particle surface are likely to be swept into the interior of the particle due to the generated vortex. Fresh metal is always available on the particle surface, resulting in enhanced particle reactivity.

Surface tension difference between formed liquid oxide and liquid metal may promote isolated spherical nodules of oxides within metal. Espie (Ref 19) has reported the formation of non-equilibrium wüstite nodules in iron particles after direct current (dc) plasma spraying (Ref 19). It was concluded that the nodules

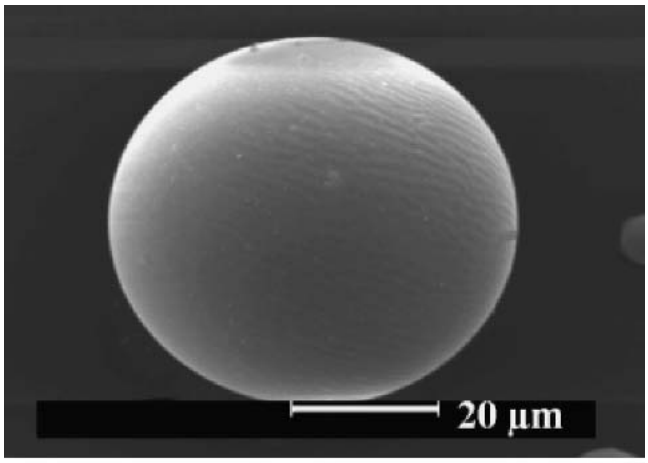

(a)

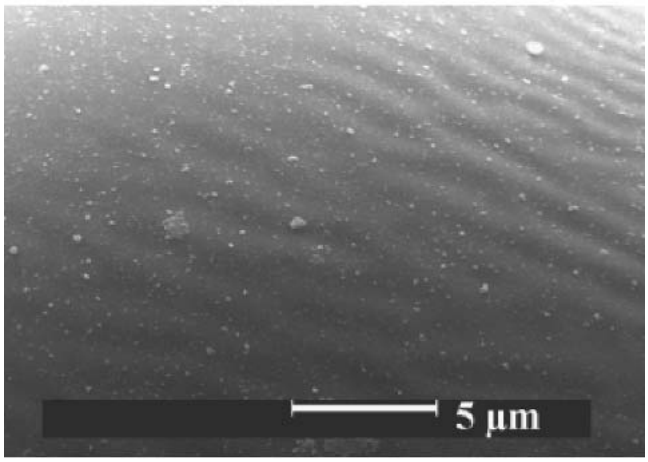

(b)

Fig. 7 Convective movement effect on the surface of the particle collected at 50 mm standoff distance (I = 550 A, Ar-H_2 = 45 to 15 slm, anode nozzle ID = 7 mm)

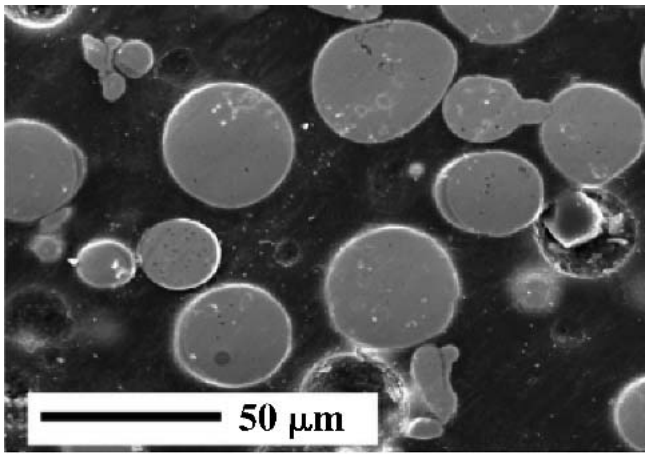

(a)

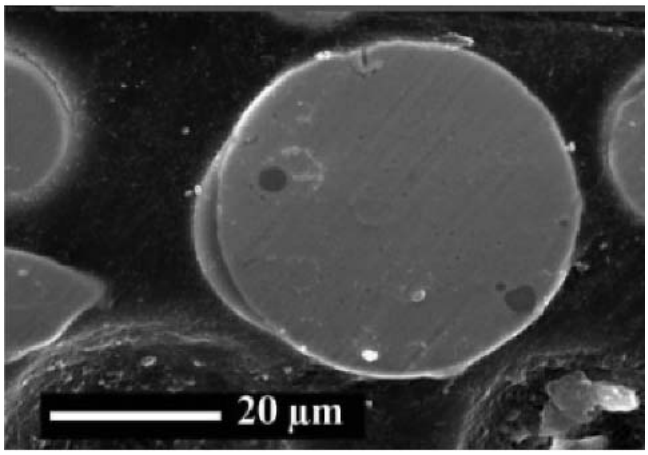

(b)

Fig. 8 Collected Metco particles after spraying by a dc plasma torch with a 6 mm ID anode nozzle (I = 550 A, Ar-H_2 = 45 to 15 slm, z = 100 mm)

Table 3 Mössbauer parameters from the spectra of collected Techphy particles shown in Fig. 12(b)

Phases	Isomer shift (δ), mm/s	FWHM/2 (Γ/2), mm/s	Quadrupole splitting (ΔE_q), mm/s	Magnetic splitting (ΔE_M), Tesla
Austenite	−0.187	0.108	0.111	0
$Fe_{3-x}Cr_xO_4$	0.867	0.110	1.640	0

FWHM, full width at half maximum

were formed due to the difference in surface energies of liquid metal and oxide.

Outside the plasma jet core, the velocities and temperatures of the plasma and particles converge to same values reducing the relative Re number. The kinematic viscosity of the plasma undergoes a rapid decay causing convective movements and oxide mass transfer from particle surface to cease. Convective oxidation and formation of nodules can, therefore, occur only within the first 40 to 50 mm downstream of the nozzle exit in standard plasma conditions. Classic diffusion-based surface oxidation becomes the dominant mechanism in the plasma plume at farther distances.

Metco particles collected after spraying using a 6 mm internal diameter anode, exhibited oxide caps (Fig. 8). The accumulation of oxide toward the tail of particles can be explained by considering the density and surface tension differences between molten metal and oxide that forms outside the plasma jet core along with the drag force on particles. While spraying mechanofused 316L steel and alumina powder, Ageorges and Fauchais (Ref 27) reported alumina entrainment in the tail of particles that were sufficiently heated. These authors have suggested that the density difference between steel and alumina could cause this segregation.

Under the same plasma conditions, smaller particles would attain a higher temperature and velocity and lower viscosity (varying as $\mu_0 \exp [E/kT]$) that can promote the entrainment of the oxide toward the tail in a cap form. Compared with smaller Techphy particles, Metco particles have much lower temperature (only a few hundred degree over their melting point) and velocity in the plasma jet, according to calculations. Conse-

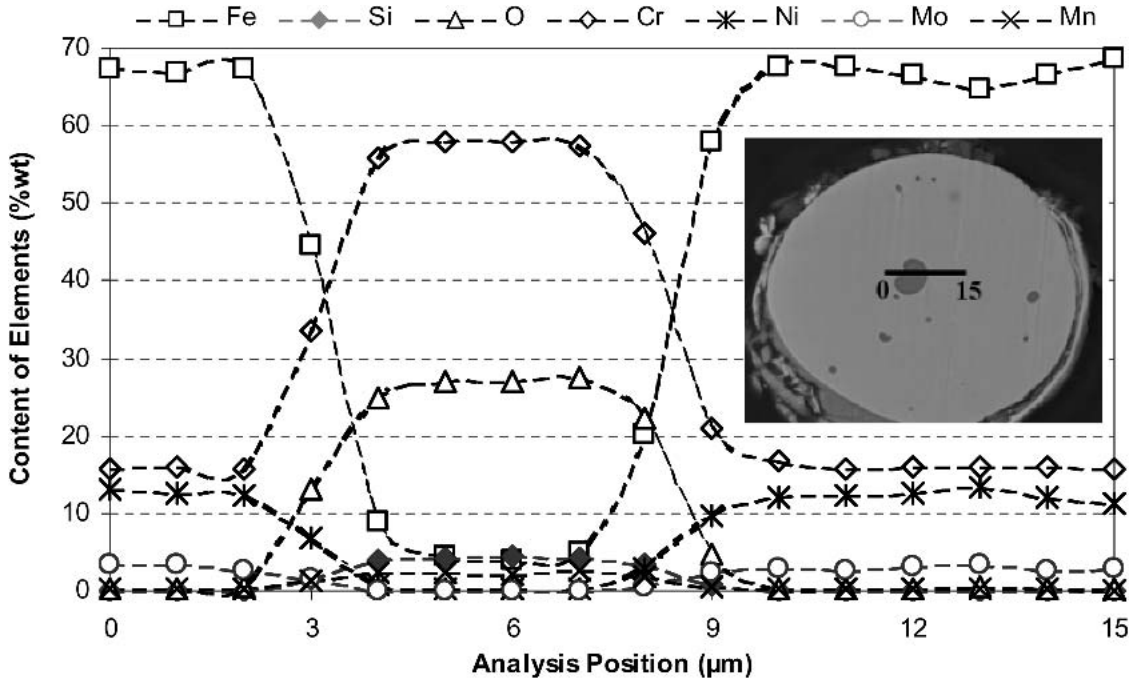

Fig. 9 Microprobe analysis along the black line of a Techphy particle collected after spraying

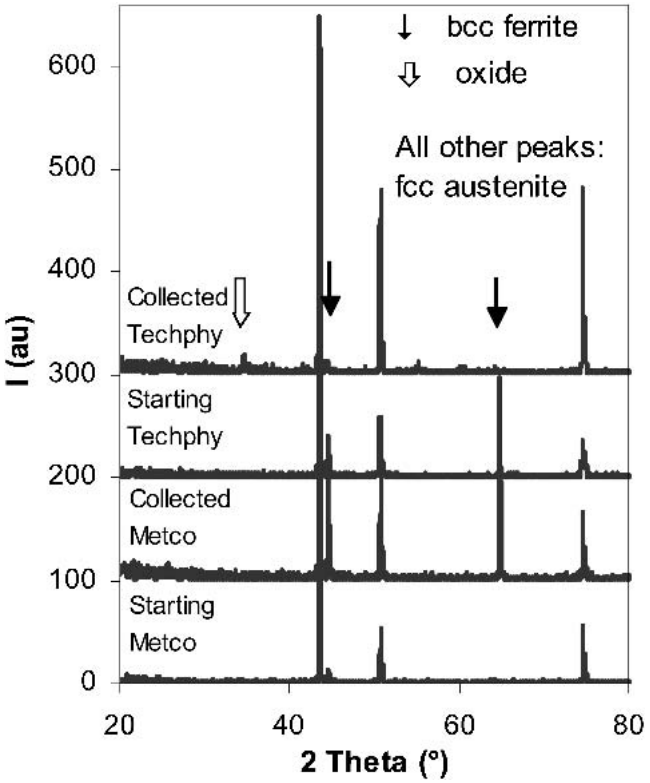

Fig. 10 XRD curves of feedstock and collected Techphy and Metco powders

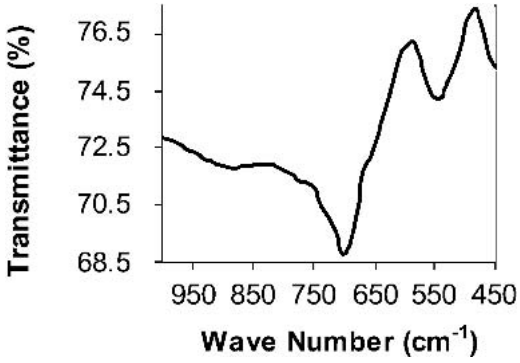

Fig. 11 FTIR spectrum of collected Techphy particles (Ref 18)

quently, their viscosity is higher and Re is lower than those of Techphy particles decreasing the $\upsilon_i = \upsilon_{plasma}/\upsilon_{particle}$. Metco particles, therefore, exhibit entrained oxide caps only if they are sprayed under conditions that would promote higher υ_i and particle Re as observed experimentally.

Microprobe analysis (Fig. 9) presents a precise elemental analysis of a Techphy particle cross section. The central area represents the oxide nodule, whereas the ends of the curve correspond to the base metal. In the oxide nodule, a significantly higher mass percentage of chromium, oxygen, silicon, and manganese can be noticed, whereas Fe content decreases considerably, and Ni and Mo are negligible.

Figure 10 shows XRD curves of feedstock and collected Techphy and Metco particles. A new peak at $2\theta = 32°$ along with a weak secondary peak at 37.5° appeared for collected powders. Three oxide phases, including CrO, Cr_2O_3, and $FeCr_2O_4$, have their major peaks corresponding closely to 2θ values. Other phase analysis techniques were, therefore, used to characterize the formed oxides.

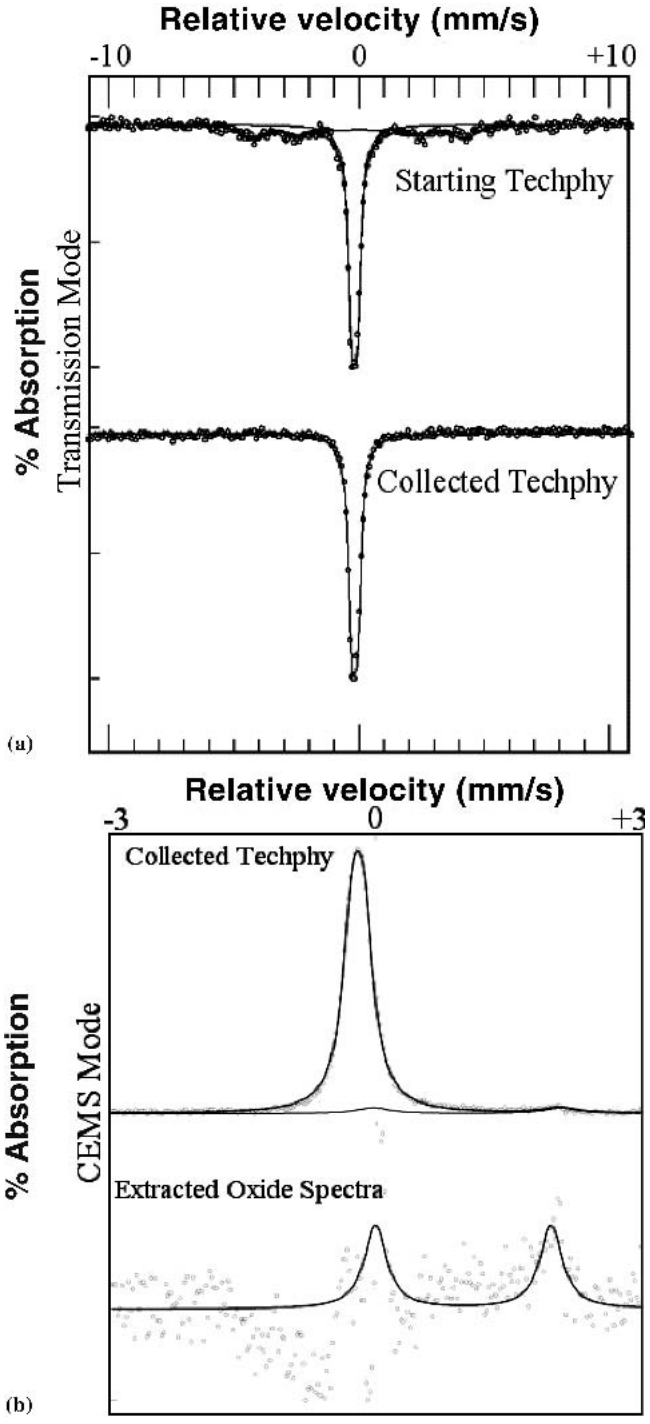

Fig. 12 Mössbauer spectra of (a) feedstock and collected Techphy powders in transmission mode and (b) collected powder in CEMS mode

The significant zone of a FTIR spectrum of collected Techphy particles is shown in Fig. 11. Two bands in the spectrum, located at 701 and 539 cm^{-1}, correspond to the stretching modes of Fe-O for iron situated in tetrahedral and octahedral sites (Ref 28). Substituting Cr atoms for Fe in octahedral sites of inverse spinel structure of Fe_3O_4, giving $Fe_{3-x}Cr_xO_4$, results in shifting of these bands toward higher wave numbers and the shifting follows a linear relationship with x value (Ref 29). For $FeCr_2O_4$ ($x = 2$), for example, these bands are located at 714 and 548 cm^{-1}, respectively. In collected Techphy particles, a spinel-type $Fe_{3-x}Cr_xO_4$ can be concluded as the major oxide phase by FTIR spectroscopy. Collected Metco particles exhibited similar spectrum.

Besides XRD and FTIR, Mössbauer spectroscopy was used to verify the results. Oxide phase analysis was not possible by transmission-mode-Mössbauer-spectroscopy, probably due to lower oxygen content in collected particles and only austenite was detected (Fig. 12a). While employing this technique, Volenik et al. (Ref 28) were able to characterize only the in-flight formed oxide in high-Cr steel powder after dissolution of the metallic phase. Conversion electron Mössbauer spectroscopy (CEMS) was, therefore, later used in the current work. Besides austenite, a doublet of a ferrous chromium oxide in the nonstoichiometric form of $Fe_{3-x}Cr_xO_4$ (Fig. 12b) was measured. The Mössbauer parameters of the presented spectrum are listed in Table 3. Subtracting the CEMS spectra of feedstock powder from the collected powder, the oxide phase doublet was mathematically extracted and is presented in Fig. 12(b). From FTIR and Mössabuer spectroscopy, the value of x was determined to be between 1.56 and 1.90.

4. Conclusions

Oxide formation and oxidation mechanisms of APS stainless steel 316L particles were studied in this work and the following conclusions can be drawn:

- The in-flight oxidation occurs in two distinct areas: in the core of plasma jet and in its plume. Convective oxidation and diffusion-controlled oxidation appeared to be the principal mechanisms in the former and latter plasma zones respectively.
- Convective movements in the liquid droplets may be induced where plasma to particle kinematic viscosities ratio is greater than 50 and the particle Re is higher than 20, conditions likely to occur in the plasma jet core. The surface oxide or oxygen dissolved at the particle surface formed in this region can be entrained in the liquid core by convective movements, and oxide nodules are formed. The fresh liquid metal is continuously renewed at the surface promoting higher particle reactivity.
- Convective movements in the particle end in the plasma plume zone and classic diffusion-based surface oxidation dominates. The formed oxide covers the surface of particles and the reaction rate decreases. The oxide formed on the surface of the particle in the plasma plume may become segregated in a cap form if liquid metal and the oxide have high Re and low viscosity.
- In-flight reactions give metastable oxides. Oxide nodules with mixed oxide of Cr, Fe, Mn, and Si as cations were detected. Spinel type $Fe_{3-x}Cr_xO_4$ ($1.90 > x > 1.56$) was the characterized major oxide phase.

Acknowledgments

The authors would like to thank Prof. B. Hannoyer of University of Rouen, France, for helping with Mössbauer and FTIR

spectroscopy and Dr. L. Bianchi of CEA, France for oxygen content measurements by the LECO technique.

References

1. O. Lagnoux, "Atmospheric Plasma Spraying by a dc Torch. Study of the Air Entrainment and Its Influence on the Particles and Coatings Oxidation," Ph.D. Thesis, University of Limoges, France, 1999 (in French).
2. E. Pfender, J. Fincke, and R. Spoores, Entrainment of Cold Gas into Thermal Plasma Jets, *Plasma Chem. Plasma Proc.,* Vol 11 (No. 4), 1991, p 529-543
3. P. Cheang, Quantitative Analysis of Thermally Sprayed Coatings using Backscattered Electron Imaging, *Thermal Spray Industrial Applications,* C.C. Berndt and S. Sampath, Ed., ASM International, 1994, p 715-720
4. J.R. Fincke, R. Rodriquez, and C.G. Pentecost, Measurement of Air Entrainment in Plasma Jets, *Thermal Spray Research and Applications,* T.F. Bernecki, Ed., ASM International, 1990, p 45-54
5. O. Lagnoux, J.F. Coudert, K. Wittman, and P. Fauchais, Study of Air Entrainment within dc Plasma Jet, *Thermal Spray: Surface Engineering via Applied Research,* C.C. Berndt, Ed., ASM International, 2000, p 71-77
6. A. Denoirjean, O. Langnoux, P. Fauchais, and V. Sember, Oxidation Control in APS: Comparison Between Ar-He-H_2 and Ar-H_2 Mixtures, *Thermal Spray: Meeting the Challenges of 21st Century,* C. Coddet, Ed., ASM International, 1998, p 809-814
7. V. Gourlaouen, F. Remy, J.M. Leger, and J. Sattonnet, Influence of Plasma Gas (Spral 22, Ar-H_2) and Impurities (O_2, H_2O) on the Electrode Lifetime During Spraying, *Thermal Spray: Meeting the Challenges of 21st Century,* C. Coddet, Ed., ASM International, 1998, p 797-801
8. A. Vardelle, P. Fauchais, and N.J. Themelis, Oxidation of Metal Droplets in Plasma Sprays, *Thermal Spray Science and Technology,* C.C. Berndt and S. Sampath, Ed., ASM International, 1995, p 175-180
9. K. Volenik, F. Hanousek, P. Chraska, J. Ilavsky, and K. Neufuss, In-flight Oxidation of High-Alloy Steels During Plasma Spraying, *Mater. Sci. Eng. A,* Vol 272, 1999, p 199-206
10. V.V. Sobolev, and J.M. Guilemany, Mechanisms of Oxidation of Thermally Sprayed Coatings, *Tagungsband Conference Proceedings,* E. Lugscheider and R.A. Kammer, Ed., DVS Deutscher Verband für Schweißen, Germany, 1999, p 45-50
11. G. Espie, P. Fauchais, B. Hannoyer, J.C. Labbe, and A. Vardelle, Study of the In-Flight Oxidation of Iron Particles during the APS—Effect of Dissolved Oxygen on the Wetting onto Ceramic Substrates, *Advanced Materials-99,* A.Q. Khan, N. Ahmad, A. Haq, K. Hussain, M.A. Khan, and A.A. Mazhar, Ed., Dr. A.Q. Khan Research Laboratories, Kahuta, Pakistan, 1999, p 423-429
12. H. Ageorges and P. Fauchais, Oxidation of Stainless Steel Particles with and without an Alumina Shell During Their Flight in a Plasma Jet, *High Temp. Mater. Proc.,* Vol 4, 2000, p 323-337
13. V. Palka, M. Brezovsky, J. Ivan, and J. Sith, Identification of the Oxides in Plasma Sprayed APS Coatings of NiCrAlY Type, *Thermal Spray: International Advances in Coatings Technology,* C.C. Berndt, Ed., ASM International, 1992, p 537-542
14. P. Fauchais, A. Vardelle, and B. Dussoub, Quo Vadis Thermal Spraying?, *J. Thermal Spray Technol.,* Vol 10 (No. 1), 2001, p 44-66
15. P. Siitonen, T. Kinos, and P.O. Kettunen, Corrosion Properties of Stainless Steel Coatings Made by Different Methods of Thermal Spraying, *Thermal Spray Industrial Applications,* C.C. Berndt and S. Sampath, Ed., ASM International, 1994, p 105-110
16. P. Sahoo and G.W. Goward, On the Suitability and Application of MCrAlY Coatings under Various Operation Conditions, *Thermal Spray Science and Technology,* C.C. Berndt and S. Sampath, Ed., ASM International, 1995, p 539-544
17. S.E. Hartfield-Wunsch, and S.C. Tung, The Effect of Microstructure on the Behavior of Thermal Spray Coatings, *Thermal Spray Industrial Applications,* C.C. Berndt and S. Sampath, Ed., ASM International, 1994, p 19-24
18. K. Volenik, V. Novak, J. Dubsky, P. Chraska, and K. Neufuss, Properties of Alloy Steel Coatings Oxidized During Plasma Spraying, *Mater. Sci. Eng. A,* Vol 234-236, 1997, p 493-496
19. G. Espie, "Oxidation of Iron Particles in a d.c. Plasma Jet Flowing in Air. Influence on Coating Properties," Ph.D. Thesis, University of Limoges, France, 2000 (in French)
20. A.A. Syed, P. Denoirjean, A. Denoirjean, J.C. Labbe, P. Fauchais, and B. Hannoyer, Oxidation at Different Stages in Stainless Steel Coatings, *Progress in Plasma Processing of Materials 2003,* P. Fauchais, Ed., Begell House, 2003, p 465-474
21. M.A. Vardelle, A.C. Leger, P. Fauchais, and D. Gobin, Monitoring Particle Impact on a Substrate during Plasma Spray Process, *NATO Series E: Appl. Sci.,* Vol. 282, 1995, p 95-121
22. P.G. Boswell, Solidification Models for High Cooling Rates, *Metals Forum,* Vol 2 (No. 1), 1979, p 40-54
23. J.F. Harper, and D.W. Moore, The Motion of a Spherical Liquid Drop at High Reynolds Number, *J. Fluid Mech.,* Vol 32, 1968, p 367-379
24. S. Prakash, and W.A. Sirignano, Liquid Fuel Droplet Heating with Internal Circulation, *Int. J. Heat Mass Transfer,* Vol 21, 1978, p 885-895
25. G.K. Batchelor, On Steady Laminar Flow with Closed Streamlines at Large Reynold Number, *J. Fluid Mech.,* Vol 1, 1958, p 177-190
26. G. Espie, A. Vardelle, J.C. Labbe, and P. Fauchais, Control of the Oxidation Phenomena during Atmospheric Plasma Spraying of Pure Iron, *Thin Solid Films,* 2003, in press
27. H. Ageorges, and P. Fauchais, Plasma Spraying of Stainless-Steel Particles Coated with an Alumina Shell, *Thin Solid Films,* Vol 370, 2000, p 213-222
28. K. Volenik, J. Leitner, F. Hanousek, J. Dubsky, and B. Kolman, Oxides in Plasma-Sprayed Chromium Steel, *J. Therm. Spray Technol*., Vol 6 (No. 3), 1997, p 327-334
29. K. Volenik, F. Hanousek, and B. Stauch, The Infrared Spectra of Solid Solutions of Some Iron and Chromium Oxides, *Czech. J. Phys*., Vol 31B (No 1), 1981, p 86-95